C. Syngas Interaction Studies

1. NMR Results and Magnetization Data

To examine the effect of syngas adsorption on the catalysts, a series of Cu/Co/Cr and Cu/Fe/Zn samples were prepared following protocol (a). After reduction H_2 was outgassed while reducing the temperature to 250°C. At this temperature CO was admitted for thirty minutes and while continuously flowing CO the temperature was reduced to room temperature and the samples were sealed under negative pressure. The NMR spectra of Co containing samples are presented in Figure 14.

NMR lines of the hydrocarbon selective catalysts (Cu/Co<1) are confined to the normally expected cobalt region (212-221 MHz) with minimal scattering. This suggests that cobalt essentially remains structurally unaffected due to the presence or absence of CO and that the gas-metal interaction is relatively weak and the absorption process could be more physical in nature. However, as the copper content increases beyond 50%, we find new lines occurring consistently at higher frequencies when CO is adsorbed on the catalyst. This indicates that the gas-metal interaction (CO-Co) leads to significant modifications in the cobalt 4s-3d charge distribution. These catalysts are reported to be alcohol and methanol selective by IFP [38]. The lines persist even after desorption of CO. It seems that the chemisorption process predominates in these catalysts. It appears that strong gas-metal interaction promotes alcohols/methanol production while weak interactions are conducive for hydrocarbon production.

FIGURE 11 **NMR FREQUENCIES OF CU/CO CATALYST**

Effect of CO Adsorption

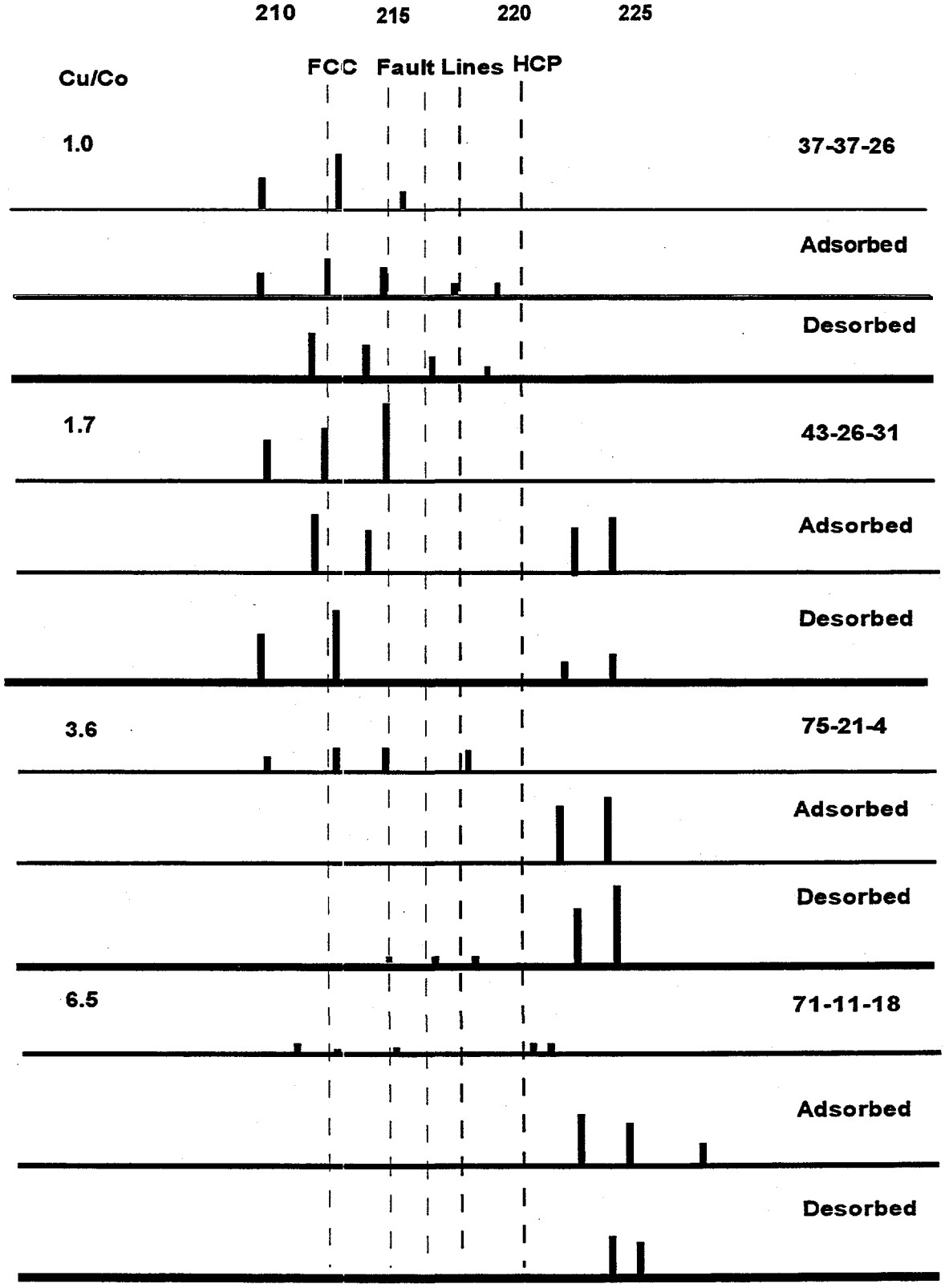

The effect of CO adsorption on the saturation magnetization of the catalysts is presented in Tables 6 (Cu/Co/Cr) and 7 (Cu/Fe/Zn). An examination of the magnetic moments of the three ferromagnetic metals and their 3d electronic structures: Fe ($3d^6$ - 218 emu/g), Co ($3d^7$-161 emu/g) and Ni ($3d^8$-54 emu/g) indicates that the magnetic moment decreases as the 3d electron density increases. For all catalysts with Cu/Co < 2 (Table 6), the magnetic moment of the CO adsorbed catalyst is lower than that for the catalyst. This suggests that there could be charge transfer from carbon monoxide to cobalt and this might be conducive for the production of hydrocarbons. However, as the copper content increases (Cu/Co > 2), alcohol and methanol selective catalysts, the magnetic moment of the CO adsorbed catalyst is higher than that for the catalyst. This indicates a reverse charge transfer from cobalt to carbon monoxide. This observation shows a clear link between the selectivity and magnetic character and the nature of syngas interaction with the catalyst.

In all the iron samples analyzed (Table 7), the magnetic moment of the CO adsorbed catalyst is significantly less than that for the catalyst. Again, this is indicative of charge transfer from carbon monoxide to iron. Unlike Cu/Co/Cr catalysts, this feature is independent of Cu/Fe ratio. This leads us to believe that all the Cu/Fe/Zn catalysts studied are likely to be hydrocarbon selective.

The last column in both tables presents the magnetization data of the CO desorbed samples. Desorption of CO was carried out by simply outgassing the samples over night for nearly 18 hours at room temperature. Both Co and Fe catalysts, consistently show a significant further drop in the magnetic moment. This further drop in the magnetic moment may be indicative of the possibility of enhancement in metal carbide formation.

TABLE 6
MAGNETIZATION DATA ON Cu/Co/Cr CATALYSTS

		SIGMA (emu/gCo)		
SAMPLE ID	Cu/Co	Cu/Co/Cr	Cu/Co/Cr+CO	Cu/Co/Cr+CO DESORBED
8-71-21	0.11	87.2	69.9	64.10
17-78-5	0.22	117.0	83.6	37.10
37-37-26	1.00	17.0	14.2	12.20
58-29-13	2.00	30.7	33.4	28.90
54-22-24	2.50	6.0	19.6	9.91
74-21-5	3.50	28.3	71.9	50.76
71-11-18	6.50	DID NOT REACH SATURATION		

TABLE 7
MAGNETIZATION DATA ON Cu/Fe/Zn CATALYSTS

		SIGMA (emu/gFe)		
SAMPLE ID	Cu/Fe	Cu/Fe/Zn	Cu/Fe/Zn+CO	Cu/Fe/Zn+CO DESORBED
8-71-21	0.11	223.4	83.5	42.18
17-78-5	0.22	164.6	82.9	79.09
37-37-26	1.00	154.6	78.9	40.48
58-29-13	2.00	135.5	66.2	26.19
54-22-24	2.50	142.7	64.5	19.87

In summary, this study clearly establishes that changes in selectivity character of the catalyst are associated with corresponding changes in the magnetic character and that the nature of the charge transfer between the adsorbate and adsorbent influences both the catalytic and magnetic properties. At low copper concentrations (hydrocarbon selective catalysts), though CO adsorption does not seem to produce significant changes in the hyperfine field at Co nuclear site, there occurs a drop in the magnetic moment of the catalyst. As the copper content increases beyond 50%, (alcohol and methanol selective catalysts), the hyperfine field significantly increases at the cobalt nuclear site and the magnetic moment of the catalyst also increases. In iron catalysts there is a consistent drop in the magnetic moment and seems to be independent of Cu/Fe metal ratio.

A series of a fresh batch of catalysts with Cu/Co ratio varying from 0.5 to 4.5 were prepared using co-precipitation technique. The catalysts were exposed to carbon monoxide, and a set of three typical catalysts with Cu/Co = 0.2, 1, and 37 were exposed to Syngas ($CO + H_2$) and the NMR spectra were scanned in the frequency region 210 - 230 MHz. We expected that if there occurs any electronic charge transfer between cobalt and carbon monoxide, the hyperfine field at the Co nuclear site will change producing a shift in the NMR spectral lines of cobalt. Positive and negative frequency shifts would indicate the direction of charge transfer between Co and CO.

The NMR data presented in Table 8 shows that in most of the catalysts prepared, nice crystallites were formed with no noticeable fault structures. The heat treatment procedure during precipitation, drying, calcination or reduction seems to have lead to the segregation of chromia, promoting copper-cobalt inter-metallic interaction. Generally NMR lines are shifted to higher frequencies in most of the samples. The presence or

absence of carbon monoxide made no difference to the NMR results. The second set of three samples exposed to Syngas neither show any unique features attributable to Syngas adsorption. The morphological structure of the samples seems to mask the subtle effects due to CO or CO +H_2 adsorption.

Magnetization properties of Cu/Co/Cr catalysts, prepared following co-precipitation technique, were investigated using a Digital Measurement Systems (DMS)-Vibrating Sample Magnetometer (VSM) at GSU. Several sets of samples with different Cu, Co, Cr elemental compositions were examined. The magnetization studies on all the samples were made at room temperature after different treatments such as: after reduction, after adsorption of CO, after desorption of CO, and after adsorption and desorption of Syngas (CO+H2). The complete data is presented in Table 9. The magnetization data is analyzed separately for hydrocarbon selective catalysts (Cu/Co < 1.5) and alcohol-methanol selective catalysts (Cu/Co > 1.5).

Figure 15 shows that, as Co content in the composite increases, σ (saturation magnetization) increases in hydrocarbon selective region (Cu/Co < 1.5), whereas (Figure 16) saturation magnetization decreases with increasing Co content in the composite in the alcohol-methanol selective region (Cu/Co > 1.5). The correlation coefficients (R-values) between σ and percent cobalt content, clearly indicate that Co dominance is high in Cu/Co<1.5 samples, and low in samples with Cu/Co>1.5. This supports the view that Co is the predominant player in hydrocarbon selective catalysts, while both Co and Cu play synergistic roles in alcohol selective catalysts, and Cu assumes a predominant role in methanol selective catalysts.

Figure 17 shows that, as Cu content in the composite increases σ has decreased in hydrocarbon selective region (Cu/Co < 1.5), while σ increases with increasing Cu content in alcohol-methanol selective regions (Cu/Co > 1.5) (Figure 18). These observations lead us to believe that Cu promotes Co reduction in alcohol-methanol selective region, while in hydrocarbon selective region Cu might produce $CoCu_2O_4$ type spinels which are not easily amiable for reduction.

Figures 19 and 20 show the effect of chromia on both hydrocarbon and alcohol-methanol selective catalysts. Saturation magnetization has consistently decreased with increasing Cr content in the composite. It appears that Cr in the form of Chromia essentially plays the role of a neutral support dispersing cobalt and copper uniformly.

Figure 21 shows that, as Cu/Co ratio increases, σ decreases in hydrocarbon selective region (Cu/Co < 1.5), and σ increases with increasing Cu/Co ratio in alcohol-methanol selective region (Cu/Co > 1.5) (Figure 22). This observation lends further support to the earlier inference on the role of copper in the composite.

A comparison between the saturation magnetization values of reduced samples and CO adsorbed samples presented in Table 9 indicate that CO adsorption in general decreases the magnetization in hydrocarbon selective catalysts while it leads to a slight increase in alcohol-methanol selective catalysts. This suggests that the direction of charge transfer between carbon monoxide and cobalt Co<===>CO is reversed in the two regions.

CO was physically desorbed from the adsorbed samples by placing the samples in a vacuum desiccator and evacuating continuously for several hours at room temperature. The magnetization results show no noticeable changes in the σ values between the CO adsorbed and the desorbed samples. This indicates that the adsorption process is not

physi-sorption and more of chemi-sorption in nature and that most of the CO is chemically bound to the catalyst and might have formed cobalt carbonyls.

For the sample with the highest Cu/Co ratio (sample Cu/Co/Cr - 74/2/24,Cu/Co = 37), a dual phase in the magnetization curve is observed with a small hysteresis loop near the origin and a raising paramagnetic straight line. The increased Cu content could have lead to the formation of solid solution of Co into Cu.

When we compare the σ values of CO adsorbed and Syngas adsorbed catalysts, σ value decreases when CO only is exposed. When Syngas is exposed σ values did not change significantly and remained close to the reduced sample values. It appears that the presence of hydrogen prevents strong chemical interaction between CO and Co and inhibits the formation of cobalt carbonyls.

Table 8: NMR Spectra of Cu-Co-Cr Catalysts with and without Adsorbed Carbon Monoxide and Syngas ($CO+H_2$)

								NMR SPECTRA							
SAMPLE	Cu/Co							Cu-Co-Cr Catalysts							
I.D	RATIO	210		213		215.5		217	218.4	221					
Cu/Co/Cr				FCC		------	FAULT	LINES	------	HCP					
32/64/4	0.5	210.8		213.3			216.1		218.4	220.9	222.5	223.3			
32/64/4	+CO 0.5	210.8		213.1			216			220.7	222.3				
37/37/26	1.0	211.1		213.6			216.6				221.7	223.4		225.3	
37/37/26	+CO 1.0	211.1		213.6								223.7		225	
43/28/29	1.5	211.6		213.8								223.7			
43/28/29	+CO 1.5	211.2		213.8								223.7			
58/29/13	2.0	211.1		213.6								223.9			
58/29/13	+CO 2.0			213.7								223.8			
54/22/24	2.5											223.7			
54/22/24	+CO 2.5											223.7			
60/20/20	3.0	211.8		213.7								223.8			
60/20/20	+CO 3.0			213.4								223.9			
74/21/5	3.5	211	212.1	213.5	214.7		216.6	217.8				223.9			
74/21/5	+CO 3.5												224.5		
63/16/21	4.0		212.8										224.8		226.5
63/16/21	+CO 4.0		212.4										224.8		226.3
80/18/2	4.4		212.2		214.3							223	224.7		226.3
17/78/5	+CO+H2 .0.2	210.8		213.4			216		218.7		221.9	223			
37/37/26	+CO+H2 1.0											223.3		225	226.5
74/2/24	CO+H2 37										221.7	223.1	224.8		226.2

Table 9: Magnetization Results of Cu-Co-Cr Catalysts with and without adsorbed, desorbed CO and Syngas.

Cu-Co-Cr	Cu/Co	σ	Hc	σ (CO)	Hc (CO)	σ ($CO+H_2$)	Hc ($CO+H_2$)	σ (COd)	Hc (COd)	σ (COH_2d)	Hc (COH_2d)
17-78-5	0.2	117	672	84	463	128	429		477	126	442
37-37-26	1	40	484	15	436	35	244	12.6	449	39	252
74-2-24	37	D.P.	203	D. P.	105	D. P.	117	D. P.	145	D. P.	66
8-71-21	0.1	87	403	70	271			64	423		
32-64-04	0.5	107	299	82	328						
43-28-29	1.5	23	254	29	272						
43-26-31	1.7	47	519	5.8	380			9.2	378		
58-29-13	2	48	381	42	346			42	373		
54-22-24	2.5	65	424	19	371			10	327		
60-20-20	3	16	198	23	244			23	257		
74-21-5	3.5	73	411	70	347			68	368		
63-16-21	4	12	306	17	312			17	322		
80-18-02	4.5	76	289	105	252			97	258		

Fig. 15: Saturation magnetization vs. cobalt concentration for Cu/Co < 1.5

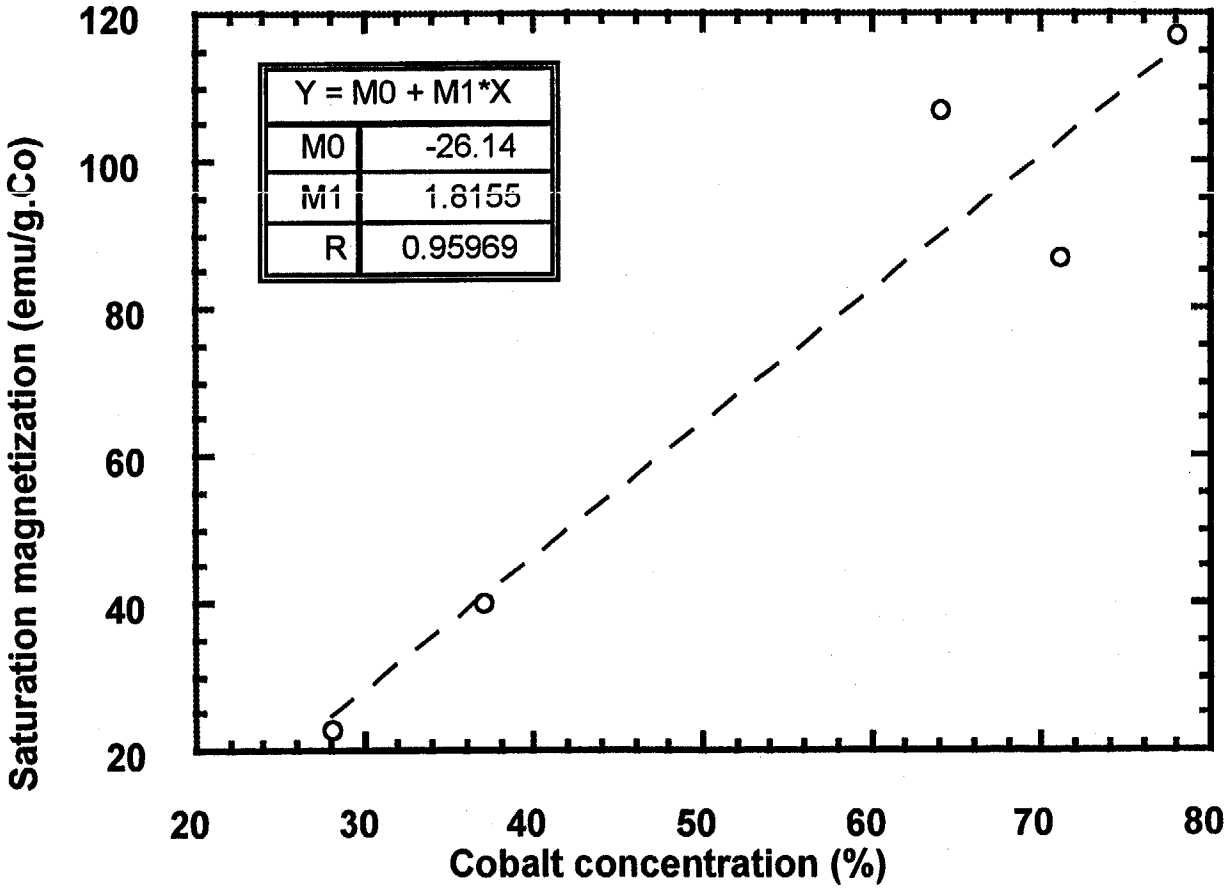

Fig. 16: Saturation magnetization vs. cobalt concentration for Cu/Co > 1.5

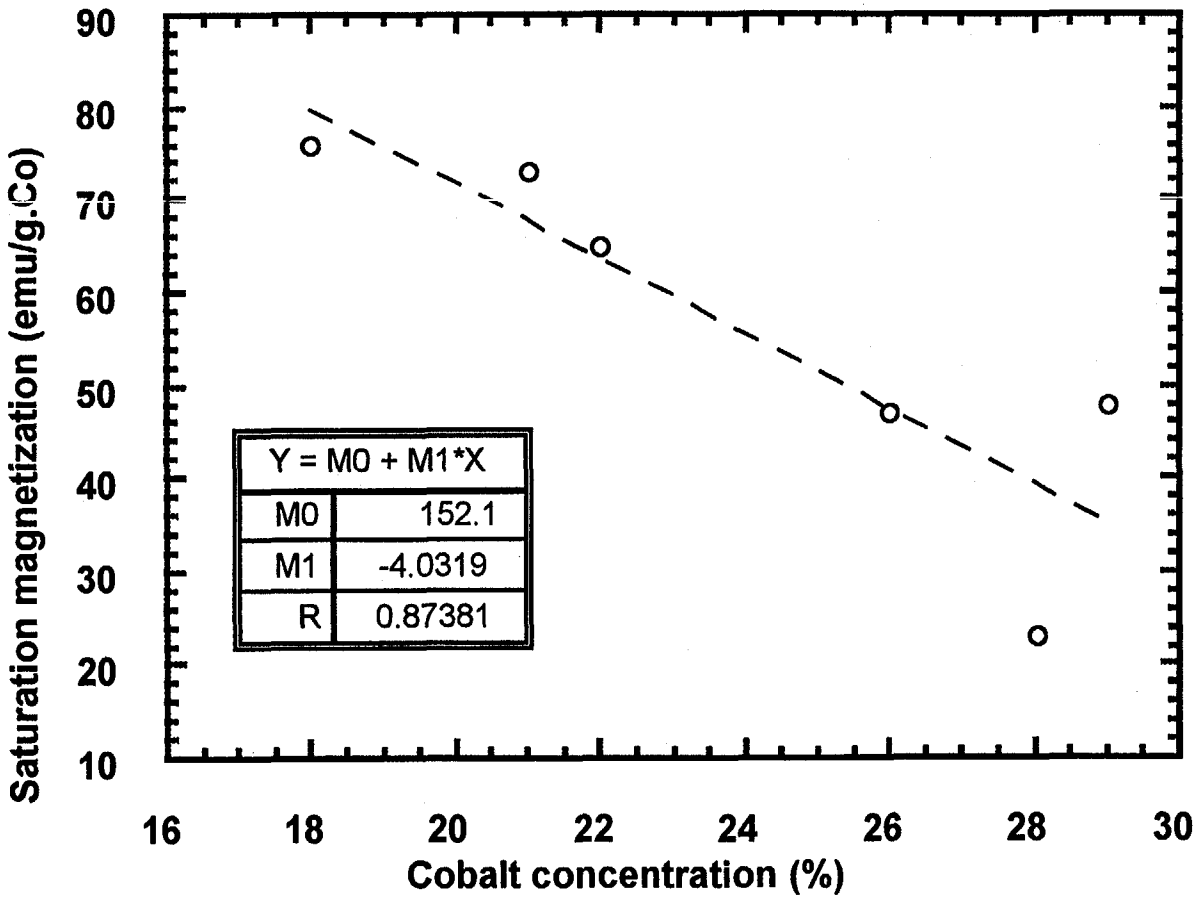

Fig. 17: Saturation magnetization vs. copper concentration for Cu/Co < 1.5

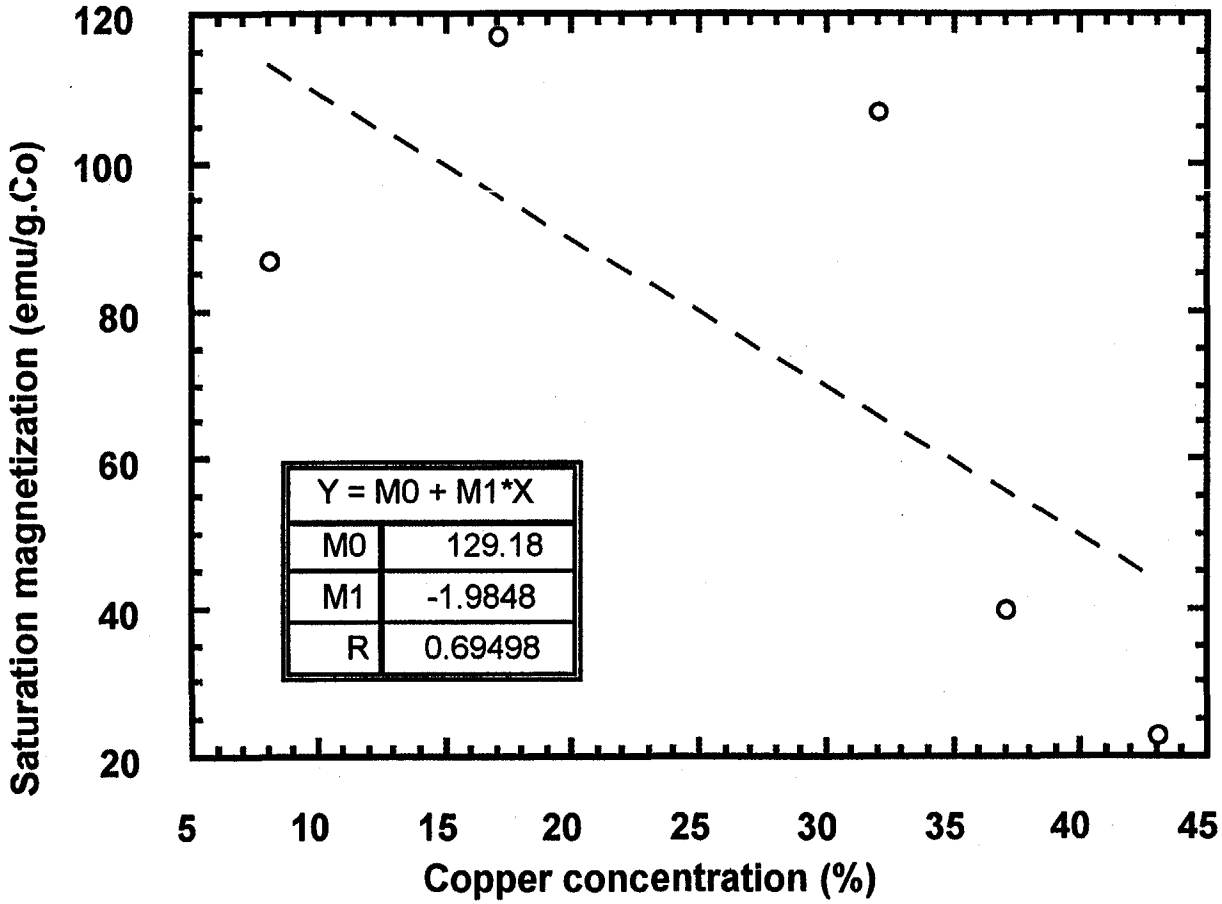

Fig. 18: Saturation magnetization vs. copper concentration for Cu/Co > 1.5

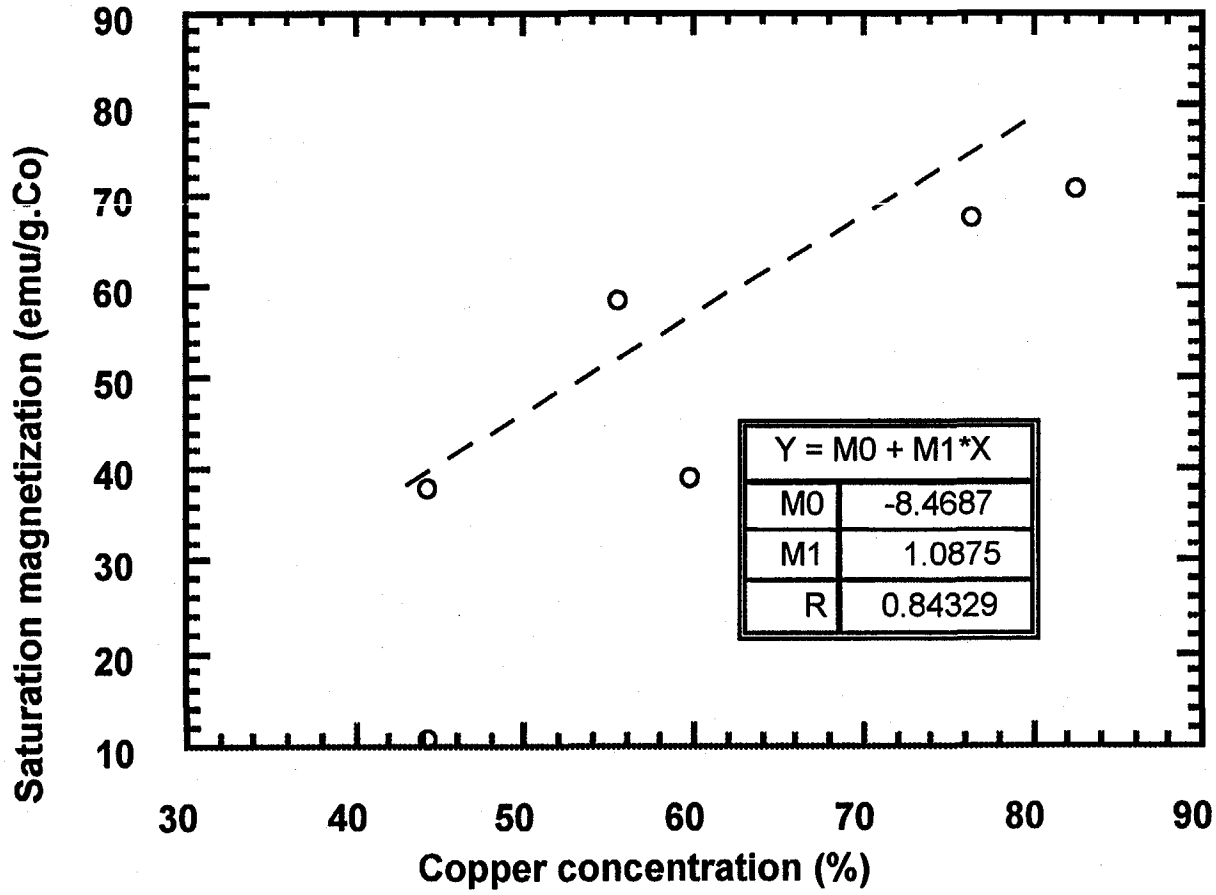

Fig. 19: Saturation magnrtization vs. chromium concentration for Cu/Co < 1.5

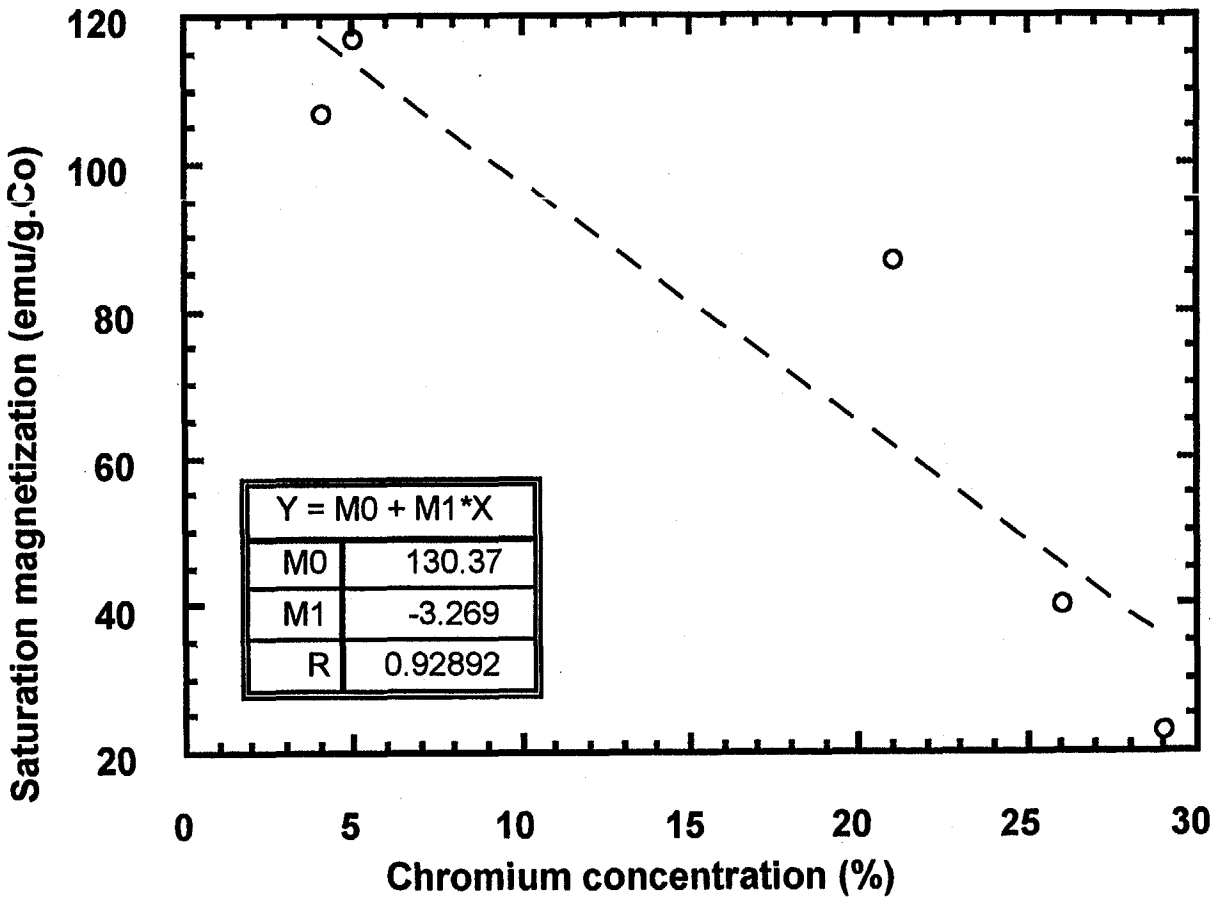

Fig. 20: Saturation magnetization vs. chromium concentration for Cu/Co > 1.5

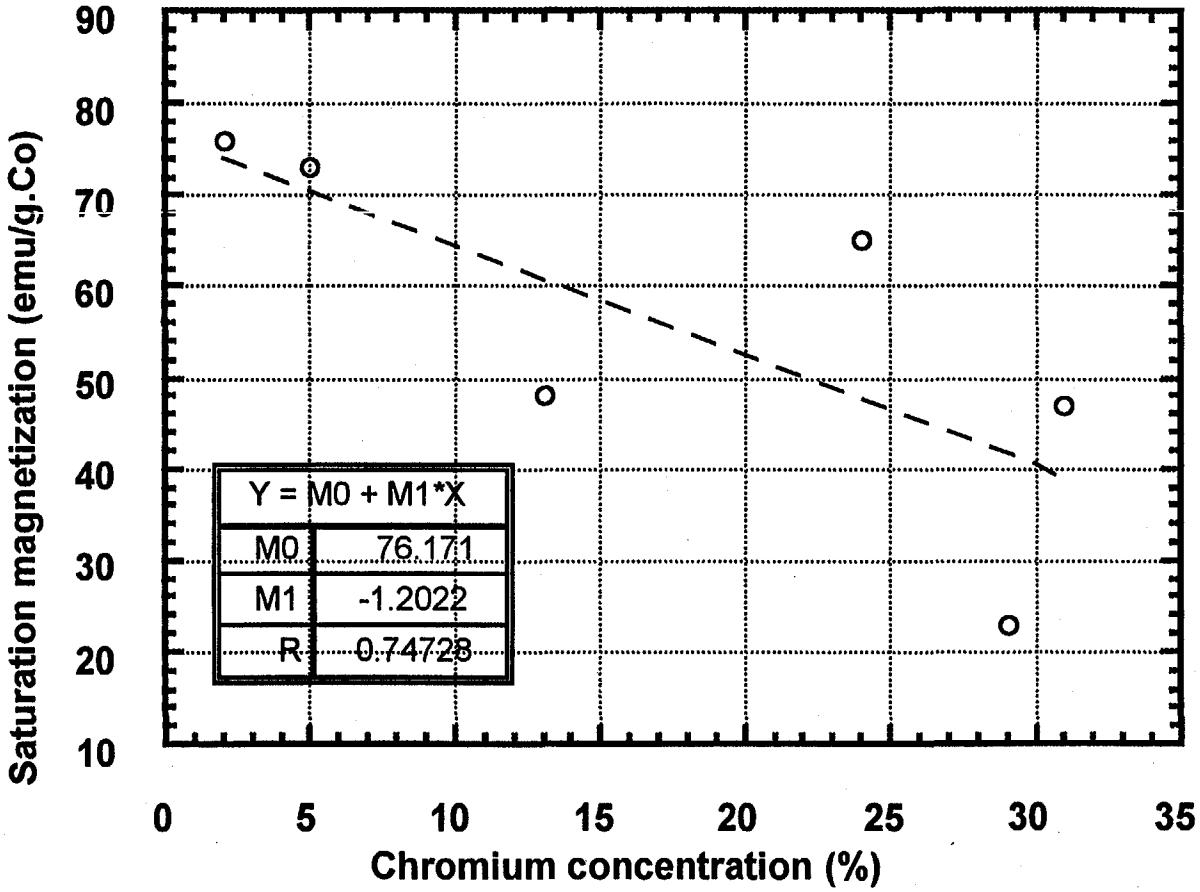

Fig. 21: Saturation magnetization vs. Cu/Co ratio for Cu/Co < 1.5

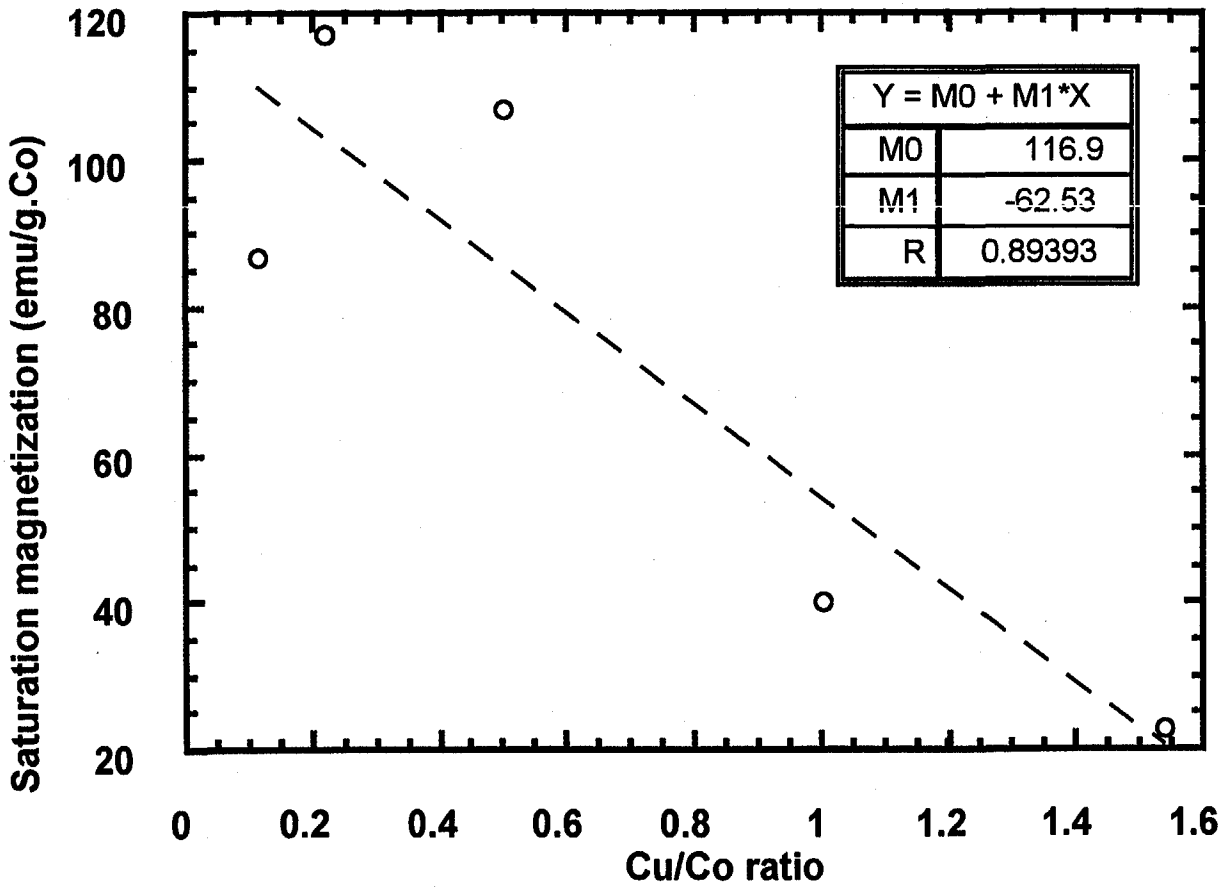

Fig. 22: Saturation magnetization vs. Cu/Co ratio for Cu/Co > 1.5

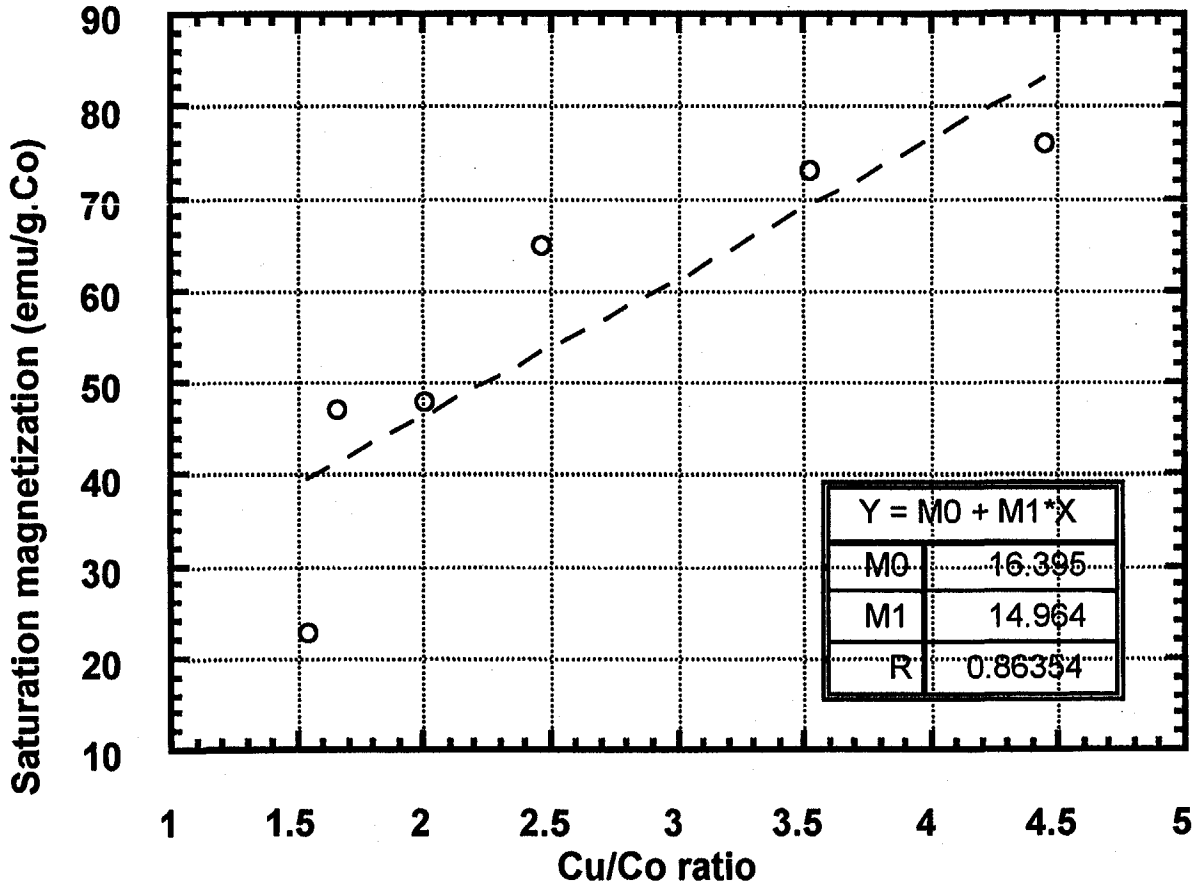

2. FTIR Studies

A comprehensive FTIR investigation on the catalysts was undertaken to unfold the picture of the gas-metal interactions. Our magnetization studies have provided valuable information on the changes in the magnetic character of the ferromagnetic metal due to CO adsorption. The FTIR results showing the effect of the adsorbate-adsorbent interactions on the stretching frequencies of the CO vibrational modes are presented in this section.

A series of 10 calcined samples with $0.5 < Cu/Co < 5$ were loaded in the sample cup of the environmental chamber of the FTIR spectrometer and were reduced in-situ before exposing to carbon monoxide. Carbon monoxide was admitted at room temperature, and while flowing CO, temperature was increased gradually in steps of 50°C and FTIR spectra were recorded at each temperature up to 250°C. We did not find any significant differences in the spectra taken at different temperatures. This suggests that gas-metal interactions might occur even at room temperature. The FTIR results are presented in Tables 10-11 and graphically depicted in Figures 23-26. Except for the single band in the region 820 - 900 cm^{-1}, all the observed bands seem to arise from four distinct metal carbonate structures as suggested by A. A. Davydov [41].

Suggested Structures:

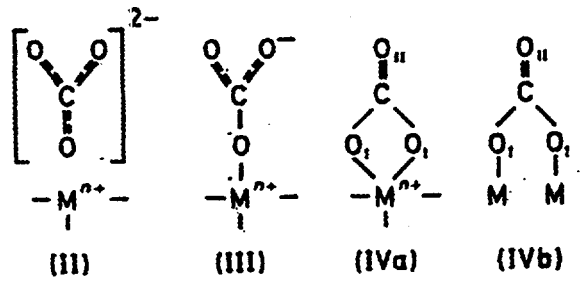

The disproportionation of carbon monoxide molecule produces $CO_{2\ ads}$ according to Boudouard reaction

$$CO_{ads} \rightarrow C^* + O^*$$

$$2CO_{ads} \rightarrow C_{ads} + CO_2$$

The CO_2 produced is believed to stabilize in the matrix in the form of a) non-coordinated carbonates (structure II), b) Mono-dentate carbonates (structure III), and c) Bi-dentate carbonates (structures IVa and b) because of the reaction

$$CO_2 + O^{2-} \rightarrow CO_3^{2-}$$

The non-coordinated carbonates generate bands in the regions: 1420-1450 cm^{-1} (νCO_3^{2-}) and 1020-1090 cm^{-1} ($\nu_s CO_3^{2-}$), monodentate carbonate structures produce bands in the region 1470-1530 cm^{-1}($\nu_{as}COO^-$), 1370-1300 cm^{-1}($\nu_s COO^-$), and 1040-1080cm^{-1} (νC-O), and bidentate carbonate structures produce bands in the region 1530-1620 cm^{-1} (νC=O), 1250-1270 cm^{-1} (ν_{as}COO), and 1020-1030 cm^{-1} (ν_sCOO) for IVA type and 1620 - 1670 cm^{-1} (νC=O), 1220-1270 cm^{-1}(ν_{as}COO), 980-1020 cm^{-1}(ν_sCOO) for IVB type. Table 10 shows the observed stretching frequencies of CO bands as Cu/Co metal ratio increases from 0.5 to 5.0. Since the 860 ± 40 cm^{-1} band consistently appears for all metal ratios of Cu/Co/Cr, and Co/Cr composite catalysts and absent in all Cu/Co composite catalysts suggests that this may be due to CO adsorption on Chromia. The bands due to structures II, III and IVb seem to be independent of the changes in the Cu/Co intermetallic ratio. The ground state electronic configuration of CO is [42]

$$1\sigma^2\ 2\sigma^2\ 3\sigma^2\ 4\sigma^2\ 1\pi^4\ 5\sigma^2$$

Broden et.al., [43] consider that the 5σ orbital of CO is essentially non-bonding with respect to the carbon and oxygen and therefore donation from the 5σ orbital to the metal should not affect greatly the **C-O** bond strength /stretching frequency. As such in these structures, the gas-metal interaction could be through the overlap of 5σ CO orbital and d orbitals of the metal. Our magnetization data support this view that charge transfer occur from CO to Co, as evidenced by the drop in the magnetic moment of Co.

The behavior of structure IVa is unique and closely parallels the magnetization results which show an increase in magnetic moment for the alcohol selective catalysts. The frequency increases from 1544 cm^{-1} for Cu/Co ≤ 1 to 1604 cm^{-1} for Cu/Co = 4 and drops for Cu/Co ratios > 4. An increase in magnetic moment is possible when the metal looses electron to the adsorbate. CO is considered as a typical π acceptor. The back donation of electrons from the metal surface orbitals to the anti-symmetric unoccupied 2π* of CO would result in lowering of the CO stretching frequency [44]. However our results show an increase in the CO stretching frequency in the alcohol region. Chini and Co-workers [45] report that when the number of metal atoms in a cluster increase, the stretching frequencies of CO also increase. The magnetization results clearly indicate that cobalt is well reduced in the alcohol selective catalysts increasing the number of metal atoms in given cluster. Hence in structure IV a the cluster mechanism seems to be responsible for observed increase in the frequencies instead of a drop as suggested by Dalman et.al. [46].

Figure 23

Vibrational frequencies of Cu-Co-Cr Composites

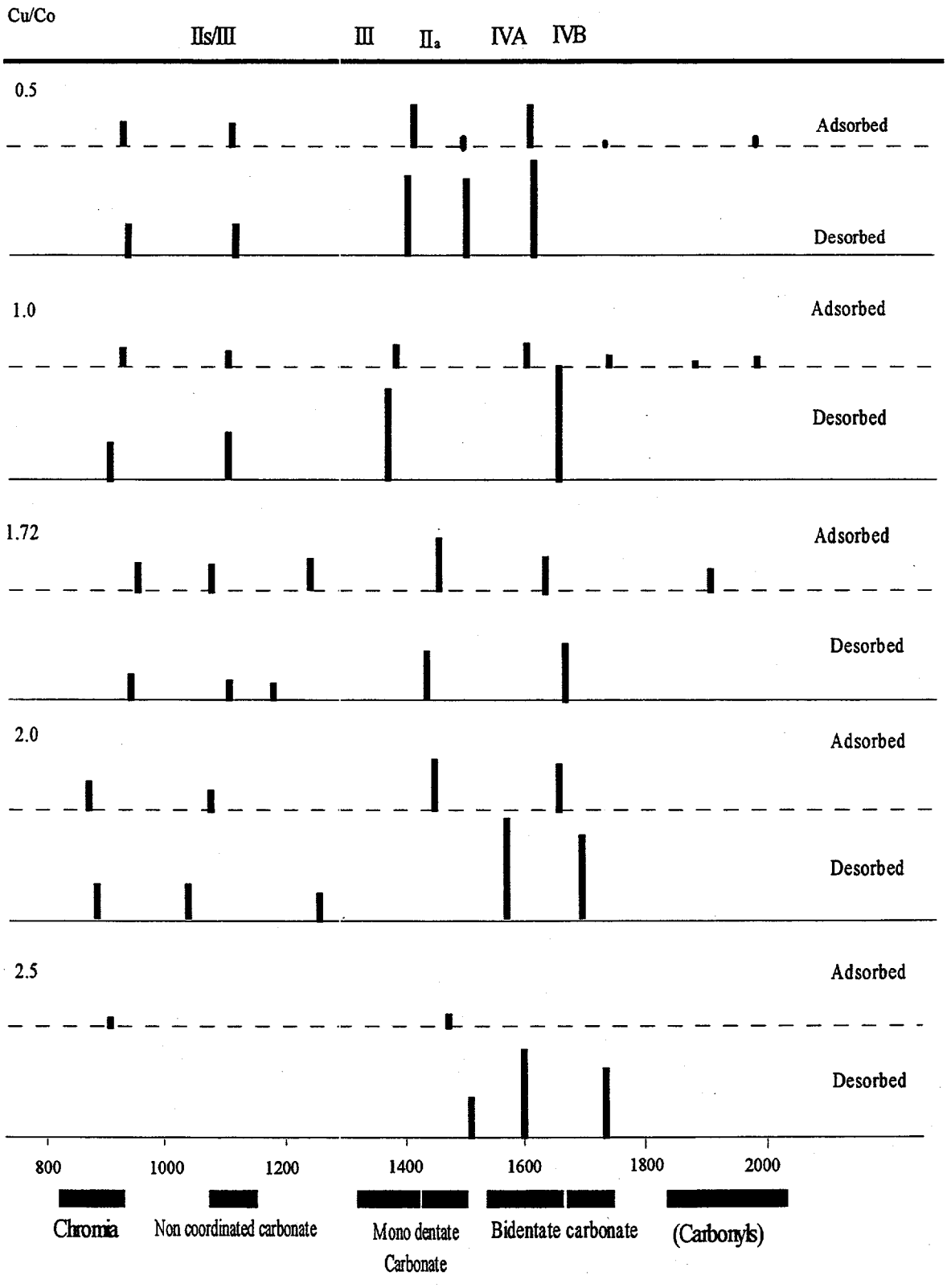

Figure 24

Vibrational frequencies of Cu-Co-Cr Composites

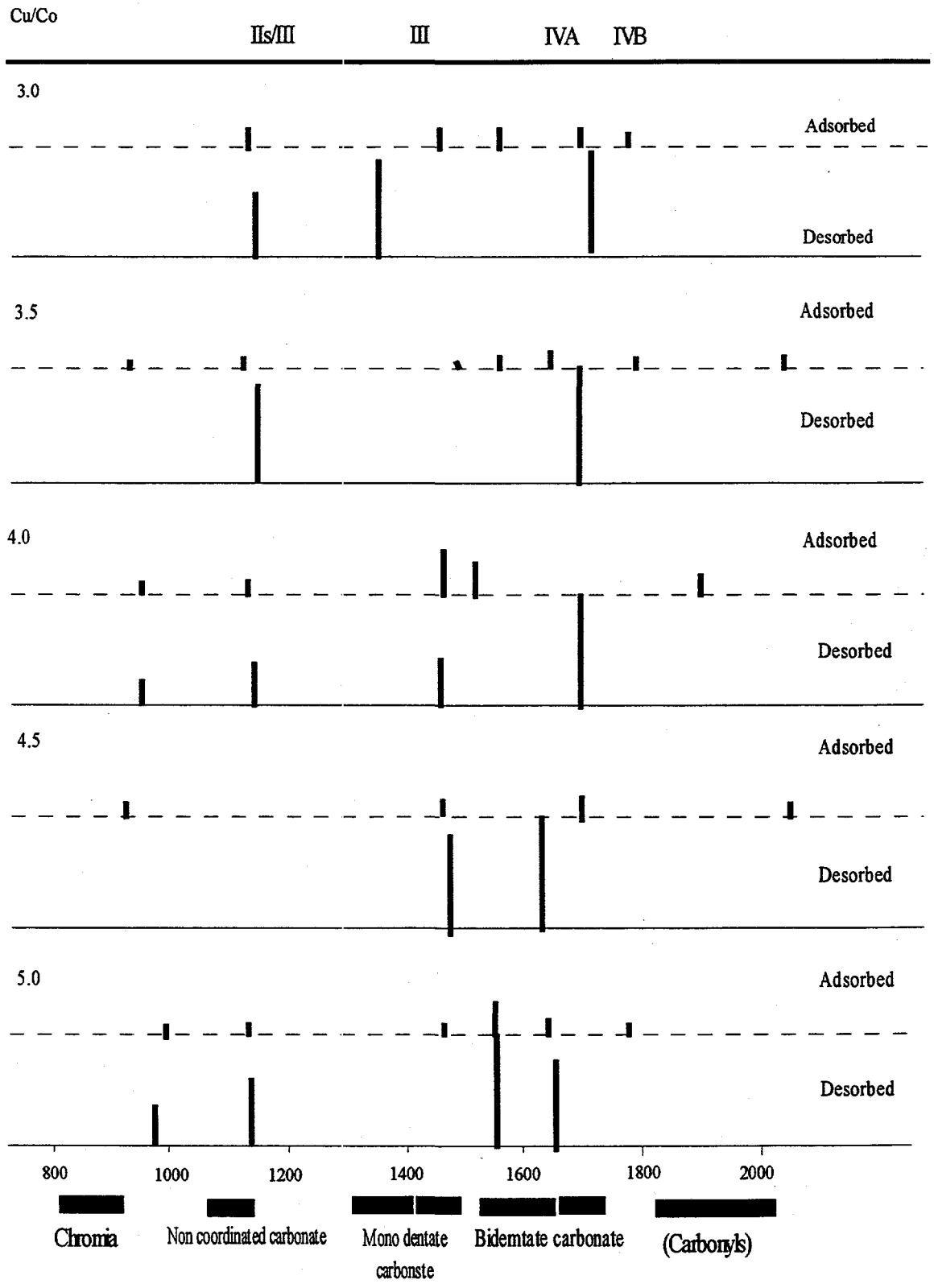

Figure 25

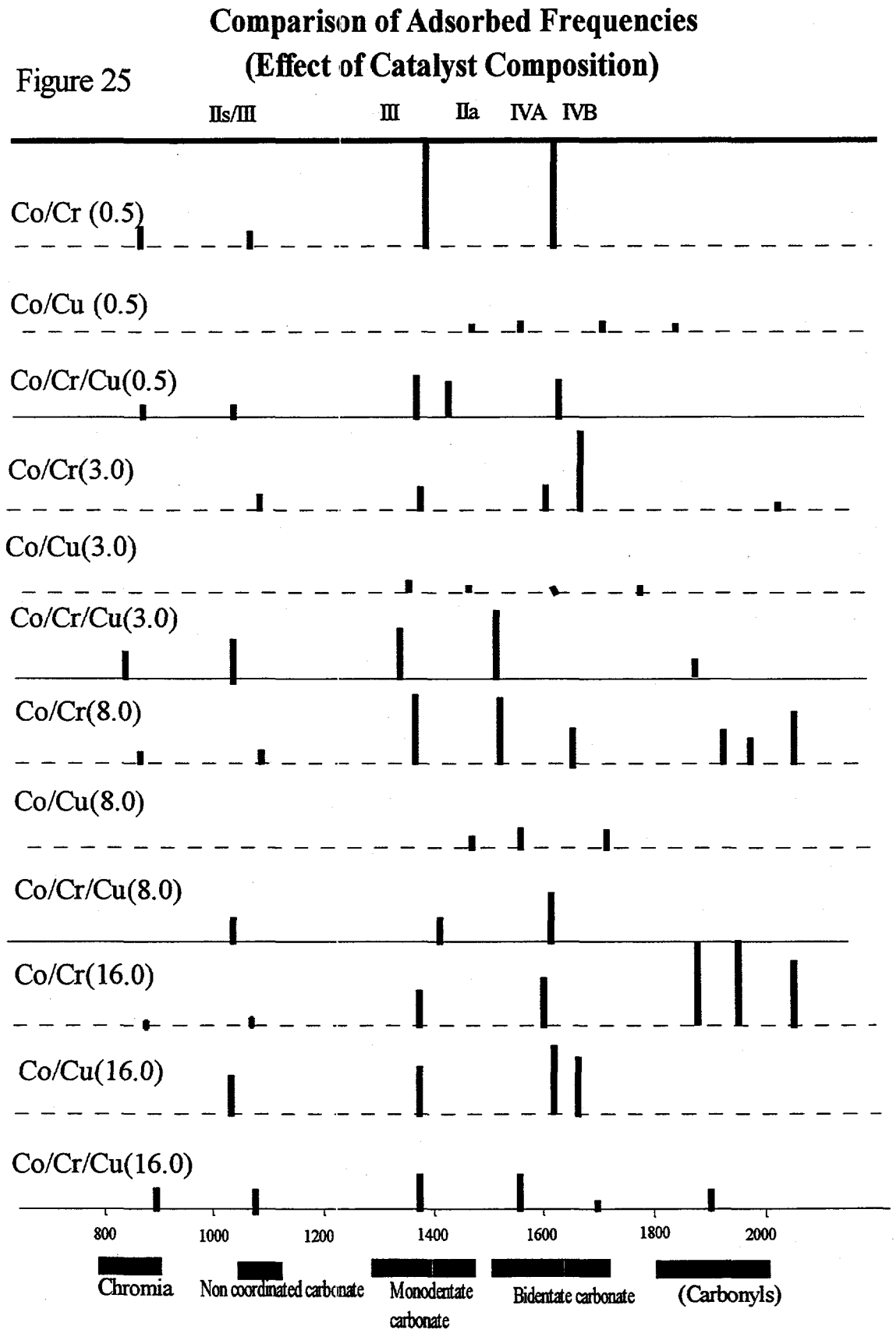
Comparison of Adsorbed Frequencies
(Effect of Catalyst Composition)
IIs/III
III
IIa
IVA
IVB
Co/Cr (0.5)
Co/Cu (0.5)
Co/Cr/Cu(0.5)
Co/Cr(3.0)
Co/Cu(3.0)
Co/Cr/Cu(3.0)
Co/Cr(8.0)
Co/Cu(8.0)
Co/Cr/Cu(8.0)
Co/Cr(16.0)
Co/Cu(16.0)
Co/Cr/Cu(16.0)
800
1000
1200
1400
1600
1800
2000
Chromia
Non coordinated carbonate
Monodentate carbonate
Bidentate carbonate
(Carbonyls)

Figure 26

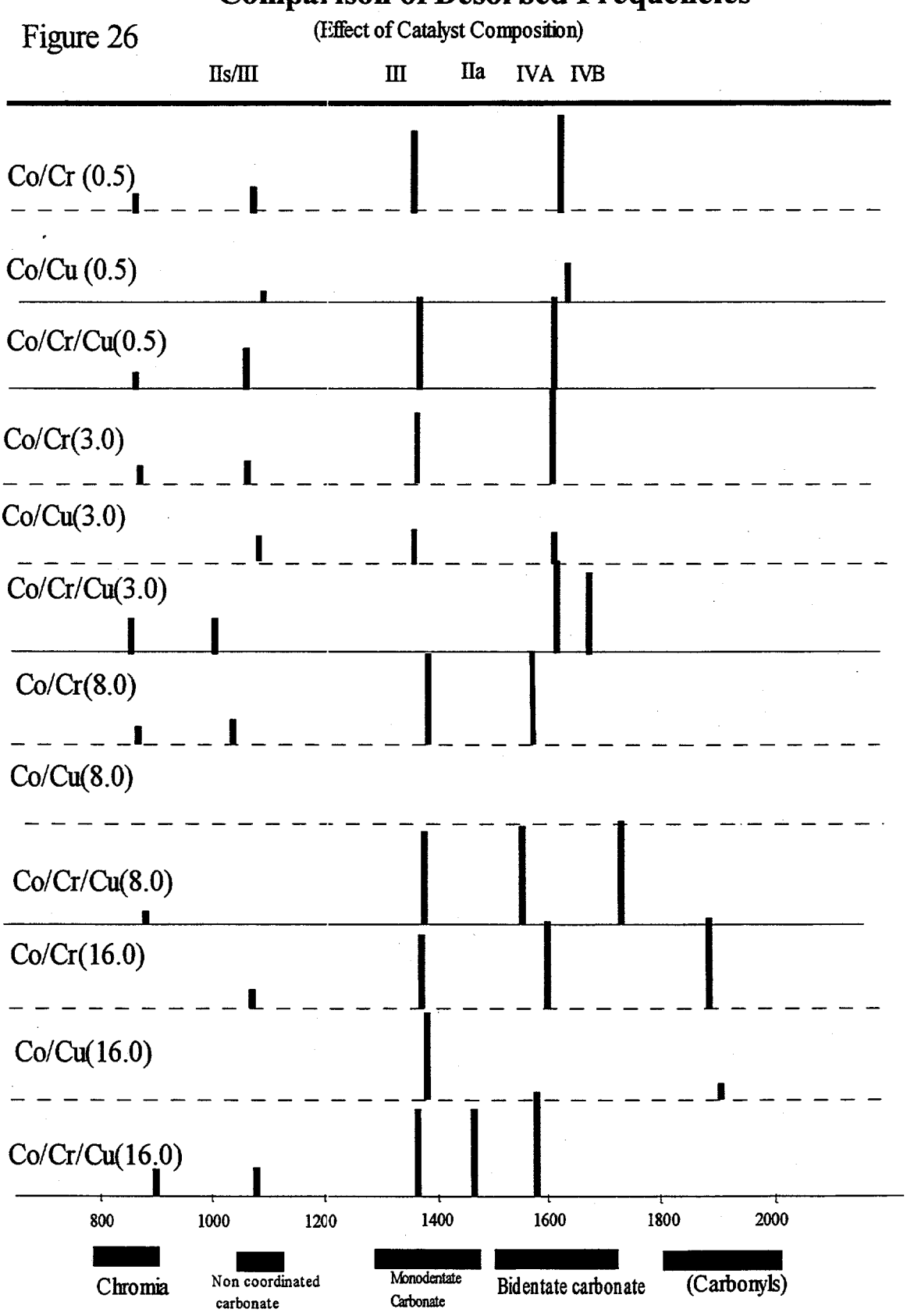
Comparison of Desorbed Frequencies
(Effect of Catalyst Composition)
IIs/III
III
IIa
IVA
IVB
Co/Cr (0.5)
Co/Cu (0.5)
Co/Cr/Cu(0.5)
Co/Cr(3.0)
Co/Cu(3.0)
Co/Cr/Cu(3.0)
Co/Cr(8.0)
Co/Cu(8.0)
Co/Cr/Cu(8.0)
Co/Cr(16.0)
Co/Cu(16.0)
Co/Cr/Cu(16.0)
800
1000
1200
1400
1600
1800
2000
Chromia
Non coordinated carbonate
Monodentate Carbonate
Bidentate carbonate
(Carbonyls)

The high frequency bands in the 1900 cm^{-1} region appear only in the hydrocarbon and methanol selective catalysts. These are the only bands that disappeared upon desorption of gaseous CO. These may be due to the cobalt carbonyl formations, $Co(CO)_4^-$, that have transiently formed due to the CO_2 stabilization on the matrix as CO_3^{2-} species according to the reaction [47].

$$2Co^{\circ} - CO + 2O^{2-} \rightarrow CO_3^{2-} + 2Co(C0)_4^-$$

This gradual disappearance is a consequence of gradual modification in the adsorbate-adsorbent interaction when the surface becomes covered by the adsorbed carbon (carbided surface). We designate these bands as physisorbed distinct from the carbonate like species bands which persist even after disorption and may be considered as resulting from the chemisorption process.

Three catalysts in the hydrocarbon, alcohol and methanol selective regions with Cu/Co ratios 0.2, 1 and 37 were chosen to study the effect of syngas ($CO + H_2$) interaction. Calcined samples were loaded into the sample cup of the DRIFT accessory and were reduced under hydrogen flow (20 cc/min) at 350°C for 18 hours. Hydrogen was outgassed while reducing the temperature to 25°C. A mixture of $CO + H_2$ (carbon monoxide and hydrogen (50/50) supplied by Gulf Coast Airgas) was admitted at this temperature. While continuing syngas flow, the temperature was increased in steps of 50°C up until 250°C and FTIR spectra were taken at each temperature. $CO + H_2$ was desorbed by evacuating the chamber at 250°C. While evacuating continuously, spectra were recorded in the reverse order. We did not observe any significant changes in the FTIR spectra due to temperature either in the adsorbed or desorbed species.

Figures 27-28 represent the FTIR spectra of the adsorbed and desorbed species of the three samples. Table 12 lists the vibrational frequencies along with their assigments. For comparison, CO adsorbed frequencies were also shown. In all the three samples fewer vibrational modes were excited in syngas exposed spectra compared to the carbon monoxide only adsorbed spectra. In the hydrocarbon selective catalyst (Cu/Co = 0.2), when catalyst exposed to carbon monoxide only, carbonyls, mono dentate, and bidentate carbonates are formed. When the catalyst is exposed to CO + H_2 only, non-coordinated carbonates are formed and all other structures are suppressed,. In the mid range (Cu/Co = 1), both monodentate and bidentate formation is not suppressed due to syngas unlike in hydrocarbons. Carbonyls formation seems to be suppressed in mid-range (alcohol selective catalyst), both in the presence of syngas or carbon monoxide. In the methanol and hydrocarbon selective regions only the presence of hydrogen seem to suppress the formation of carbonyls. Also in the methanol and hydrocarbon selective catalysts, the monodentate and bidentate carbonate formation seem to be transcient, whereas in alcohol catalysts, the bidentate carbonate formation persist even after desorption.

Table 10

Vibrational frequencies of Cu-Co-Cr Catalysts

SAMPLE I	Metal ratio Cu/Co	CO on Cr_2O_3 800-900	$\nu_s CO_3$ -/νC-O II/III 1040-1080	$\nu_s COO^-$ III 1300-1370	$\nu_{as} CO_3^{2-}$ II 1420-1450	νCO=O IV a 1530-1620	νC=O IV b 1620-1670	Carbonyls $(CO)_4^-$ 1800-2000
32-64-4	0.5	860 (879)	1056 (1058)	1358 (1344)	1434 (1446)	1544 (1556)	1673	1928
37-37-26	1.0	859 (845)	1056 (1058)	1328 (1316)	–	1544 (1598)	1673	1925
43-28-29	1.5	898 (877)	1024 (1031)	1392 (1377)	–	1580 (1603)	–	–
58-29-13	2.0	822 (834)	1020	1392 (1359)	–	1598 (1648)	–	–
54-22-24	2.5	850	–	–	1415 (1453)	– (1676,1538)	–	–
60-20-20	3.0	–	1036 (1035)	1352 (1344)	1454	1598 (1606)	1670	–
74-21-5	3.5	823 (840)	1017 (1044)	1383	1455	1539 (1591)	1688	1937
63-16-21	4.0	850 (844)	1019 (1035)	1351 (1352)	1408	1604 (1588)	–	–
80-18-2	4.5	823	–	1352 (1371)	–	1597 (1518)	–	1941
50-10-40	5.0	878 (878)	1025 (1025)	–	1445 (1445)	1541 (1545)	1672	–

Table 11
Comparison of vibrational frequencies of Co/Cr catalyst

Modes of Vib.	1			3			8			16		
	Co/Cr	Co/Cu	Co/Cr/Cu	Co/Cr	Co/Cu	Co/Cr/Cu	Co/Cr	Co/Cu	Co/Cu/Cu	Co/Cr	Co/Cu	Co/Cr/Cu
Unknown (820-900)	844 (844)	– –	850 (844)	846 (851)	– –	– (986)	849 (846)	– –	823 (936)	858 (846)	– –	860 (879)
$\nu(CO_3)^{2-}$/νC-C II III (1040-1080)	1064 (1053)	– (1075)	1019 –	1065 (1054)	– (1046)	1036 –	1056 (1056)	– –	–	1049 (1043)	1015 –	1056 (1058)
$\nu_s COO^-$ III (1300-1378)	1364 (1343)	– –	1351 (1352)	1371 (1362)	1335 (1350)	1362 (1359)	1354 (1368)	– –	1352 (1371)	1369 (1352)	1354 (1329)	1358 (1344)
$\nu(CO_3)^{2-}$ II (1420-1450)	– –	1450 (1451)	1408 –	– –	1442 –	1454 –	– –	1454 –	– –	– –	– –	1434 (1446)
νC=O IVa (1530-1620)	1599 (1605)	1535 (1535)	1604 –	1585 (1597)	1602 (1596)	1598 (1595)	1549 (1561)	1532 –	1597 –	1576 (1580	1595 –	1544 (1556)
nC=O IVb (1620-1670)	1657 –	1692 –	– –	1645 –	– –	1670 (1648)	1635 (1648)	1697 –	– –	– –	1642 –	1673 –
$\nu(CO)_4^-$ (1800-2000)	2002 –	1821 –	– –	2004 –	– –	– –	1902 1959 2031	– – –	– – –	1863 1932 2028	1883 (1884) –	– 1928 –

Figure 27: Comparison of Vibrational Frequencies of CO and CO + H2 Adsorbed Species

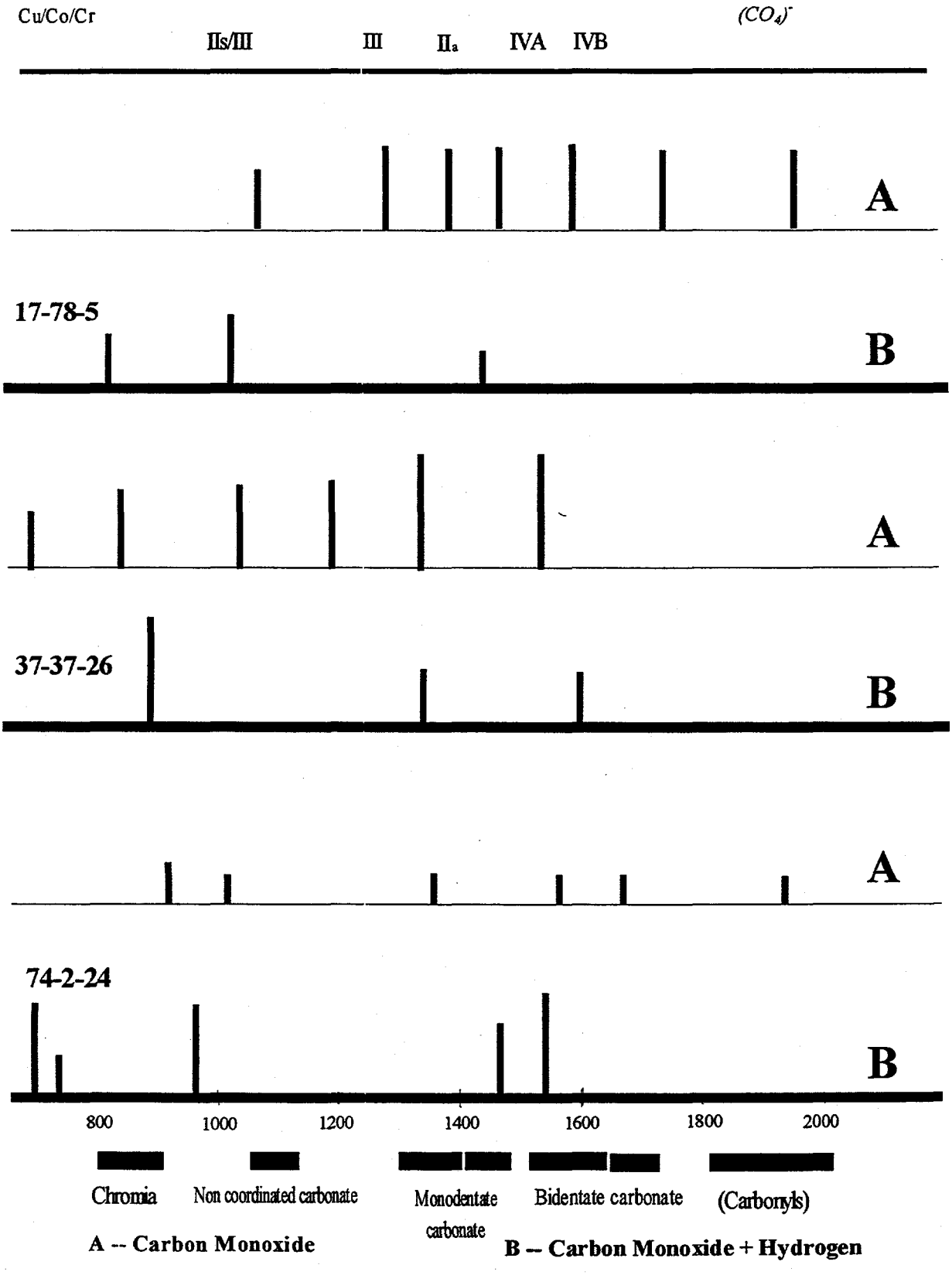

Figure 28: Comparison of Vibrational Frequencies of CO and CO + H2 Desorbed Species

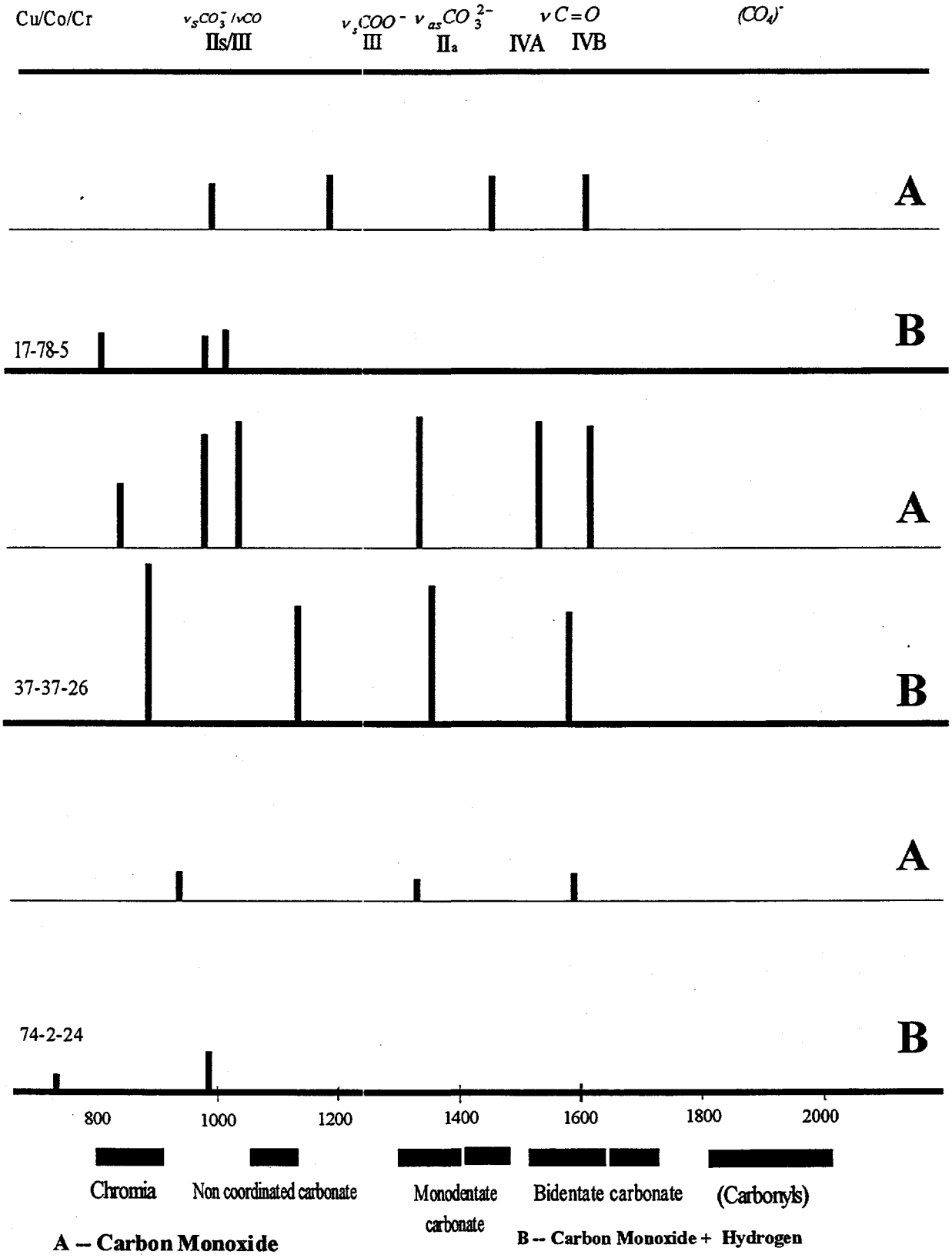

Table 12: Vibrational Frequencies of CO and CO+H_2 on Cu-Co-Cr Catalysts

17-78-5				37-37-26				74-2-24				Assignment
With CO	esorbed	CO + H_2	Desorbed	With CO	Desorbed	CO + H_2	esorbed	With CO	esorbed	CO + H_2	Desorbed	
1954	-	-	-	-	-	-	-	1931	-	-	-	Carbonyls (CO_4^-)
-	-	-	-	-	-	-	-	-	-	-	-	Carbonyls (CO_4^-)
1735	-	-	-	-	-	-	-	-	-	-	-	Carbonyls (CO_4^-)
-	1602	-	-	-	1624	-	-	1672	-	-	-	vC = 0 IV b
1585	-	-	-	1523	1542	1599	1579	1563	1587	1535	-	vCO = 0 IV a
1474	1450	1428	-	-	-	-	-	-	-	1464	-	$\nu_{as}CO_3^{2-}$ II
1380	-	-	-	1326	1349	1331	1353	1354	1326	-	-	$\nu_s COO^-$ III
1276	-	-	-	-	-	-	-	-	-	-	-	
-	1178	-	-	1185	-	-	1127	-	-	-	-	
1073	-	1024	1019	1022	1034	-	-	1018	-	-	-	$\nu_s CO_3^-$/vC-O II / III
-	989	-	981	-	980	-	-	923	936	963	983	CO on Cr_2O_3
-	-	823	822	837	844	896	885	-	-	-	-	
-	-	-	-	-	-	-	-	-	-	732	733	
-	-	-	-	691	-	-	-	-	-	698	-	